Fission properties for *r*-process nuclei

J. Erler,[1,2,3] K. Langanke,[4,5,6] H. P. Loens,[4,5] G. Martínez-Pinedo,[4,5] and P.-G. Reinhard[1]
[1]*Institut für Theoretische Physik II, Universität Erlangen-Nürnberg, Staudtstrasse 7, D-91058 Erlangen, Germany*
[2]*Department of Physics and Astronomy, University of Tennessee, Knoxville, Tennessee 37996, USA*
[3]*Physics Division, Oak Ridge National Laboratory, Oak Ridge, Tennessee 37831, USA*
[4]*GSI Helmholtzzentrum für Schwerionenforschung, Planckstr. 1, D-64291 Darmstadt, Germany*
[5]*Technische Universität Darmstadt, Institut für Kernphysik, Schlossgartenstr. 9, D-64289 Darmstadt, Germany*
[6]*Frankfurt Institute of Advanced Studies, Ruth-Moufang Str. 1, D-60438 Frankfurt, Germany*
(Received 5 December 2011; published 14 February 2012)

We present a systematics of fission barriers and fission lifetimes for the whole landscape of superheavy elements (SHE), i.e., nuclei with $Z \geqslant 100$. The fission lifetimes are also compared with the α-decay half-lives. The survey is based on a self-consistent description in terms of the Skyrme-Hartree-Fock (SHF) approach. Results for various different SHF parametrizations are compared to explore the robustness of the predictions. The fission path is computed by quadrupole constrained SHF. The computation of fission lifetimes takes care of the crucial ingredients of the large-amplitude collective dynamics along the fission path, as self-consistent collective mass and proper quantum corrections. We discuss the different topologies of fission landscapes which occur in the realm of SHE (symmetric versus asymmetric fission, regions of triaxial fission, bimodal fission, and the impact of asymmetric ground states). The explored region is extended deep into the regime of very neutron-rich isotopes as they are expected to be produced in the astrophysical *r* process.

DOI: 10.1103/PhysRevC.85.025802 PACS number(s): 21.60.Jz, 23.60.+e, 25.85.Ca, 26.30.Hj

I. INTRODUCTION

The existence of superheavy elements (SHE) above the naturally existing ones has attracted much attention in the past decades [1,2]. The topic remains of high actual interest as the new and heavier synthesized elements are added every year to the list, for a few examples from the rich list see [3–7]. Superheavy elements are also produced during the *r* process [8–10] and their properties are important in order to determine the upper end of the nucleosynthesis flow. The key question in the study of SHE is their stability against the various decay channels as α decay, β decay, and particularly spontaneous fission. This paper aims at a theoretical survey of fission lifetimes for SHE. It will establish a systematics all over the landscape of SHE from the experimentally accessible neutron poor ones to the very neutron rich species which may occur in the *r* process. Fission lifetimes will also be compared with the lifetimes for α decay. This survey is based on a theoretical description at level of a self-consistent mean field (SCMF). Such models came into practice about 40 years ago and have been steadily developed to deliver now a reliable description of nuclear structure and dynamics, for recent reviews see [10–14]. We use here in particular the Skyrme-Hartree-Fock (SHF) approach which stays in the nonrelativistic domain and employs an effective energy functional corresponding to zero-range interactions [12].

The first theoretical estimates of fission stability were performed on the grounds of the shell correction energy within phenomenologically adjusted shell model potentials [15] and studies of shell structure persist to be of high exploratory value also for self-consistent approaches [16,17]. In the realm of SHE, one finds broad islands of shell stabilization rather than the narrow and deep valleys as they are typically found for lighter nuclei [18]. The emergence of large regions of stable nuclei is, in fact, favorable for the potential experimental accessibility. The next step after estimates from the shell correction energy is to check the systematics of fission barriers in SHE. There exists a wealth of information about fission in actinide nuclei [19] which helps to probe the predictive value of the theoretical approaches, e.g., of the SHF method [20,21]. (In fact, a fission barrier was used in the calibration of one SHF functional [22].) However, comparison with experimental data requires to go beyond a pure SHF description and to take into account collective correlations (from rotation and low-energy vibration) which can modify the fission barriers by up to 2 MeV [23,24]. The systematics of fission barriers in SHE is simplified by the fact that there is only one fission barrier to be considered (as opposed to actinides with their double-humped barrier). It was found [21,25] that SHF provides estimates of islands of fission stability which are qualitatively in accordance with experiments [26–28]. The ultimate goal is, of course, to estimate the fission lifetimes directly. However, self-consistent calculations of fission lifetimes are extremely demanding and thus have come up only recently, see, e.g., [29–31] (which are mostly using still approximate masses and quantum corrections [23]) or [32] for a fully self-consistent calculation. In this paper, we employ the method as presented in [32] for establishing the systematics of fission lifetimes for all conceivable SHE. We will discuss the influence of the choice of the SHF parametrization and we will compute and compare also the lifetimes for α decay.

The paper is outlined as follows. Section II presents the formal framework for the computation of fission lifetimes. Section III discusses a variety of results on fission barriers, fission lifetimes, and a comparison with α-decay lifetimes.

II. FORMAL FRAMEWORK

A. SHF approach and pairing

The basis of the description is SHF augmented by BCS pairing. The method is widely used and well documented in the literature, for reviews see, e.g., [12,14]. We report here briefly the actual input and usage.

The mean-field state is a BCS state characterized by a set of single-particle wave functions $\{\varphi_\alpha, \alpha = 1 \ldots \Omega\}$ and corresponding BCS occupation amplitudes v_α. The SHF energy functional depends on density ρ, kinetic energy density τ, spin-orbit density $\mathbf{J}$, current $\boldsymbol{j}$, spin density $\boldsymbol{\sigma}$, and spin kinetic density $\boldsymbol{\tau}$. We use the standard form of the Skyrme functional, in some cases augmented by an isovector spin-orbit term [33]. We employ consistently the full form including the time odd currents ($\boldsymbol{j}$, $\boldsymbol{\sigma}$, $\boldsymbol{\tau}$) which play a crucial role in computing the collective masses along the fission path (see Sec. II B). For the pairing functional we use the density dependent zero-range pairing force [34,35] in the stabilized form [36] which reads in detail

$$E_{\rm pair}^{\rm (stab)} = E_{\rm pair}\left(1 - \frac{E_{\rm cutp}^2}{E_{\rm pair}^2}\right) = E_{\rm pair} - \frac{E_{\rm cutp}^2}{E_{\rm pair}}, \tag{1a}$$

$$E_{\rm pair} = \frac{1}{4}\sum_{q\in\{p,n\}} V_{{\rm pair},\boldsymbol{q}} \int d^3r \xi_q^2 \left[1 - \frac{\rho}{\rho_{0,\rm pair}}\right], \tag{1b}$$

$$\xi_q = \sum_{\alpha\in q} f_\alpha u_\alpha v_\alpha |\varphi_\alpha|^2, \quad \boldsymbol{q} \in \{\rm prot, neut\}, \tag{1c}$$

where $u_\alpha = \sqrt{1 - v_\alpha^2}$ is the pair density and f_α is a cut-off weight as defined in Ref. [37]. When proceeding along the deformation path, the pairing energy, $E_{\rm pair}$, is plagued by a possible phase transition to the breakdown of pairing which, in turn, leads to singularities in the collective mass. A widely used method to stabilize pairing against breakdown is to employ the Lipkin-Nogami recipe, see, e.g., [38]. This, however, is not always effective enough in the breakdown regime. The stabilized functional (1a) provides a much more robust scheme. We use it with $E_{\rm cutp} = 0.6$ MeV which leaves ground state properties nearly unchanged and is at the same time very efficient in suppressing singularities in the collective mass.

The form of the SHF functional is more or less prescribed by a low-momentum expansion of a fictitious underlying effective two-body interaction [39]. But the model parameters cannot yet be derived from *ab initio* methods with sufficient precision. It is customary then to adjust the parameters of the SHF functional to experimental data, mostly from ground state properties [12,14]. Steadily growing availability of data from exotic nuclei and different preferences in the choice of the fit data has led to a variety of SHF parametrizations. One needs to check the results for sufficiently different parametrizations in order to explore the predictive value of SHF calculations. We will consider the following parametrizations: SkM* [22] as a traditional benchmark because it is one of the first parametrizations delivering a quality description of nuclear ground states; SkI3 [33] which for the first time exploits the freedom of an isovector spin-orbit coupling thus simulating in this respect the situation in relativistic mean-field models; SLy6 [40] which had been developed with a bias to neutron rich nuclei and neutron matter aiming at astrophysical applications; SV-min [41] as a recent development using a large pool of semimagic nuclei which were checked to have negligible correlation effects; and SV-bas which was adjusted to the same data as SV-min with an additional constraint on nuclear matter properties (symmetry energy, isoscalar and isovector effective masses) to tune giant resonances together with ground state properties [41]. We will also show a result for HFB-14 as one representative in a large series of parametrizations derived in large scale fits biased on a comprehensive description of binding systematics, in this case referring to published data [42].

All these parametrizations employed different pairing recipes in their original definition. In order to make calculations better comparable, we use the same pairing functional (1) for all parametrizations and tune the pairing parameters ($V_{{\rm pair},p}$, $V_{{\rm pair},n}$, $\rho_{0,\rm pair}$) to the data from even-odd staggering as summarized in Ref. [41]. Such a separate adjustment for each force is crucial because the actual pairing gaps energy from an interplay of pairing strengths $V_{{\rm pair},q}$ and level density which depends sensitively on the effective mass and thus varies dramatically with the parametrization [12,14].

B. Microscopic computation of fission lifetimes

Fission represents a substantial rearrangement of a nucleus from one into two fragments. SCMF models are well suited to track this process in a least prejudiced manner. They require only one constraint to force a stretching of the system along the various stages while all other details of the rearrangements and shapes result automatically of the calculation. Actually, one uses an isoscalar quadrupole constraint because the first stages of fission develop out of large-amplitude quadrupole modes of the mother nucleus. Even this last piece of guesswork could be eliminated by using the recipes of adiabatic time-dependent Hartree-Fock (ATDHF) [23,43]. This, however, has not yet been accomplished for the very heavy systems considered here. We stay at the level of constrained SHF and employ ATDHF only for a self-consistent evaluation of the collective mass and quantum corrections [23].

Fission barriers have been discussed already in the early stages of SCMF models and have even been used as benchmark for calibration [22]. The calculation of fission lifetimes are much more involved as their computation requires not only the potential energy surface along the fission path, but also the corresponding collective masses and a safe estimate of the collective ground state correlations for the initial state. Thus, the vast majority of calculations of fission lifetimes employ the microscopic-macroscopic method which combines shell corrections with a macroscopic liquid-drop model background, see, e.g., [44,45]. Self-consistent calculations of fission lifetimes are still rare, see, e.g., [29,30], and mostly use still approximate masses and quantum corrections. On the other hand, just because the computation of fission lifetimes is so demanding they serve as extremely critical observables probing all aspects of the effective nuclear interaction, its global bulk properties as well as details of shell structure.

To calculate fission lifetimes within SHF we use the scheme as presented in Ref. [32]. We consider a fission path which evolves along axially symmetric shapes and characterize the deformation by the dimensionless axial quadrupole momentum

$$\alpha_{20} = \frac{4\pi}{5}\frac{\langle\Phi|\hat{Q}_{20}|\Phi\rangle}{\langle\Phi|r^2|\Phi\rangle}, \tag{2a}$$

$$\hat{Q}_{20} = \sqrt{\frac{5}{16\pi}}(2z^2 - x^2 - y^2). \tag{2b}$$

The steps to compute the fission lifetimes can then be summarized as:

(i) The fission path is a set of mean-field states $\{|\Phi_{\alpha_{20}}\rangle\}$ representing the stages on the way from the ground state to fission. It is generated by quadrupole-constrained SHF (complementing the mean-field Hamiltonian by a constraining potential, i.e., $\hat{h} \to \hat{h} - \boldsymbol{\lambda}\cdot\hat{\mathbf{Q}}_{20}$).

(ii) The energy expectation value corresponding to $|\Phi_{\alpha_{20}}\rangle$ yields a "raw" collective energy surface, $\mathcal{V}(\alpha_{20})$.

(iii) The collective mass, $B(\alpha_{20})$, and moments of inertia are computed by self-consistent cranking (often called ATDHF cranking) along the states $|\Phi_{\alpha_{20}}\rangle$ of the path [46].

(iv) Approximate projection onto angular momentum zero is performed using the moments of inertia and angular-momentum width.

(v) Quantum corrections for the spurious vibrational zero-point energy (ZPE) are applied (using quadrupole mass and width). The result is the ZPE corrected potential energy surface (PES), $V(\alpha_{20})$.

(vi) The collective ground state energy E_0 is computed fully quantum mechanically for the thus given collective Hamiltonian [46].

(vii) The tunneling rate W at the given ground state energy and the repetition rates T are computed by the standard semiclassical formula (known as the WKB approximation) using the quantum-corrected potential energy and collective mass (moments of inertia); the fission lifetime is finally composed from these two quantities as T/W:

$$W = \exp\left(-2\int_b^c \sqrt{\frac{V(\alpha_{20}) - E_0}{B(\alpha_{20})}}d\alpha_{20}\right), \tag{3}$$

$$T = \hbar\int_a^b d\alpha_{20}(\sqrt{B(\alpha_{20})(E_0 - V(\alpha_{20}))})^{-1}, \tag{4}$$

where the initial state would be classically bound in the interval (a, b), while the barrier extends over the interval (b, c) (see Fig. 1).

Point 6 in this list requires some explanation. The axially symmetric fission path is described by three collective degrees of freedom (deformation α_{20} and two rotation angles) while the full collective quadrupole dynamics calls for the five-dimensional Bohr Hamiltonian. In order to be consistent with the whole fission path, a three-dimensional collective dynamics for quadrupole motion was derived which is restricted to axially symmetric shapes. The method employs the norm and overlap kernel of the topological Gaussian overlap approximation [47,48] and relies on the direct solution of the collective Schrödinger equation (see [46]), rather than establishing a (reduced) Bohr Hamiltonian.

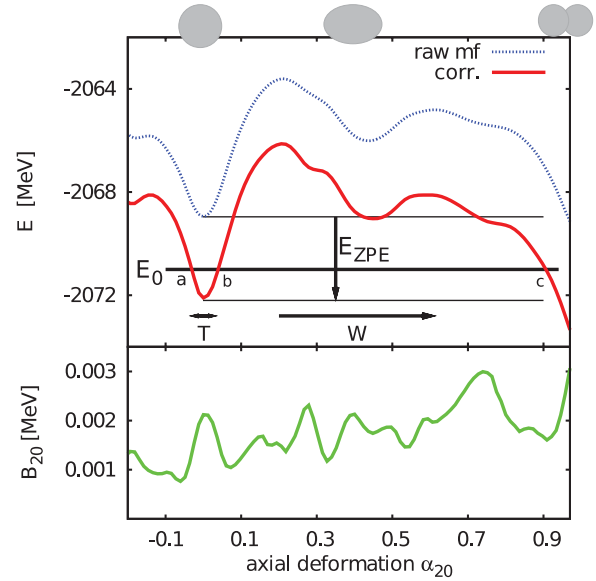

FIG. 1. (Color online) Upper panel: Raw potential energy surface (PES) $\mathcal{V}(\alpha_{20})$ and ZPE corrected PES $V(\alpha_{20})$ for ^{290}Sg. The energy E_0 of the collective ground state is indicated by a heavy horizontal line. The points a, b, and c indicate the three crossing points of the E_0 line with the collective potential $V(\alpha_{20})$. Tunneling and repetition rates W and T are also indicated. Lower: Inverse collective mass $B_{\alpha_{20}}$ calculated by a self-consistent cranking scheme (ATDHF cranking). Schematic nuclear shapes are sketched.

Figure 1 illustrates the collective parameter functions along the axially symmetric path for the superheavy element ^{290}Sg which are necessary for calculation of the fission half-lives. As can be seen in Fig. 1 the collective mass fluctuates strongly so it can hardly be approximated by some constant or weakly changing collective mass.

As mentioned above, all calculations are performed in axial symmetry but allowing for reflection asymmetric shapes. This breaking of reflection symmetry becomes crucial in the outer region beyond the fission barrier. The ground states and the (first) barrier are usually associated with reflection symmetric shapes with few exceptions as discussed in the Appendix. Breaking of axial symmetry toward triaxial shapes can occur in the barrier region. One knows from actinides that triaxial shapes can lower the barriers by about 0.5–2 MeV [25,49]. Such lowering is missing in axially symmetric calculations. The present results are thus to be understood as providing an upper limit for barriers and lifetimes.

III. RESULTS AND DISCUSSION

A. Benchmark

Lifetimes can be derived by the calculation scheme developed above. Figure 2 shows fission lifetimes for four

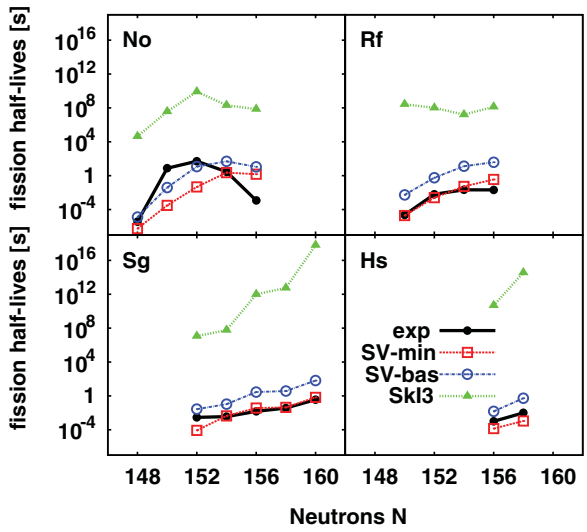

FIG. 2. (Color online) Fission lifetimes of the isotopes No, Rf, Sg, and Hs computed with three different Skyrme parametrizations, as indicated, and compared with data from [3,6,7,50–54].

chains at the lower end of SHE. Three SHF parametrizations are compared. SkI3 which has a rather low effective mass ($m^*/m = 0.58$) does not perform so well. This holds similarly for all forces with low effective masses. The results from the recent parametrizations SV-min and SV-bas which have effective mass $m^*/m = 0.95$ and 0.9 provide a more satisfying agreement taking into account that an order of magnitude description is already a success for the extremely subtle observable of fission lifetime. For the No isotopes, the agreement is acceptable in the average but there appears a strong deviation in the isotopic trend. This mismatch stems probably from the axial approximation and could well be explained by a strong isotopic change of the triaxial lowering of the barrier.

Figure 3 shows experimental and calculated results on fission barriers (lower panel) and lifetimes (upper panel) for a few selected SHE, but now extending to heavier elements and comparing more SHF parametrizations. The SHE represent two groups, one at the lower side (already included in Fig. 2) and another one with much heavier nuclei at the limits of present days data. The span of predictions from the various Skyrme forces is huge in all cases in spite of the fact that all these parametrizations provide a high-level description of nuclear ground state properties along the valley of stability. The variation of predictions may be a welcome feature as it provides additional selection criteria for a SHF parametrization. There remains, however, a problem when looking at the trend from the lighter side (Rf, Sg, Hs) to the heavier elements ($Z = 112$, 114). All parametrizations produce a wrong trend of the predictions from the lower to the upper region. Barriers and lifetimes are well reproduced in the lower group by SV-min and SV-bas. But these parametrizations underestimate the barrier heights and lifetimes for the upper group [59]. The problem persists even with a more flexible density dependence of the Skyrme functional [60]. It is also unlikely that triaxiality, ignored here, could help. It would worsen the situation for SV-min and SV-bas and the possible

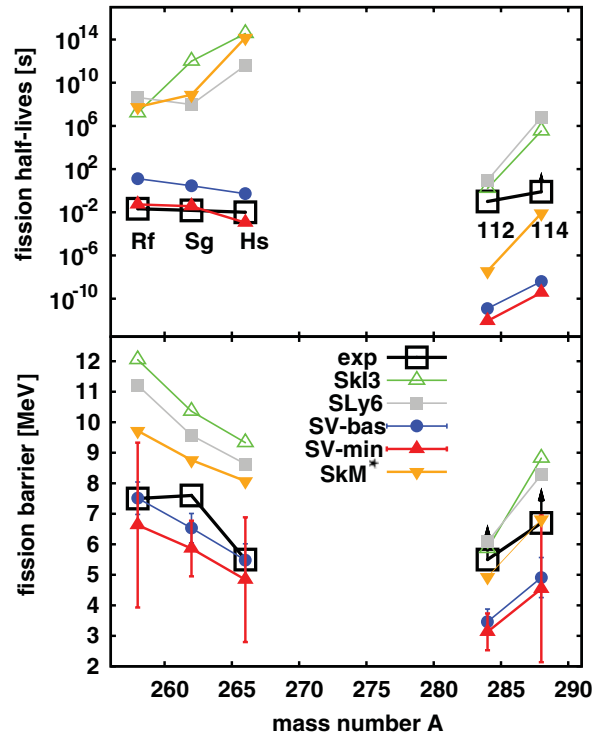

FIG. 3. (Color online) Fission barriers (lower) and lifetimes (upper) for two groups of experimental known superheavy elements. Compared are results from a variety of Skyrme parametrizations with experimental data [5,50,55–58]. The error bars on the barriers for SV-min are the uncertainties in the extrapolation as implied in the least-squares fits of the parametrization [41].

lowering about 0.5–2 MeV is insufficient to bridge the gap for the other parametrization. One has to keep in mind, however, that an experimental determination of lifetimes and barriers for the heaviest elements is a very demanding task and the data may not yet have reached their final stage such that the mismatch should presently not be overinterpreted. In any case, we can expect from modern parametrizations as, e.g., SV-min a pertinent picture of the systematics of fission lifetimes for SHE.

B. Fission topologies

When going through the variety of SHE, one encounters much different shapes of the fission landscape. Four different situations can be distinguished as shown schematically in Fig. 4:

Panel a: shows a case where the potential energy surface has a strong oblate minimum and optionally a secondary prolate minimum. It is thus assumed that the fission path is going through the triaxial plane [61]. In fact, we have seen from fully triaxial calculations that in most cases already the ground state acquires some triaxiality. Therefore, it is not possible to make reliable predictions using an axial code in such cases. No fission barriers and lifetimes will be shown for this region in the following sections.

Panel b: shows a PES for the case of a reflection asymmetric ground state which occurs in two region in $88 \leqslant Z \leqslant 96$ and

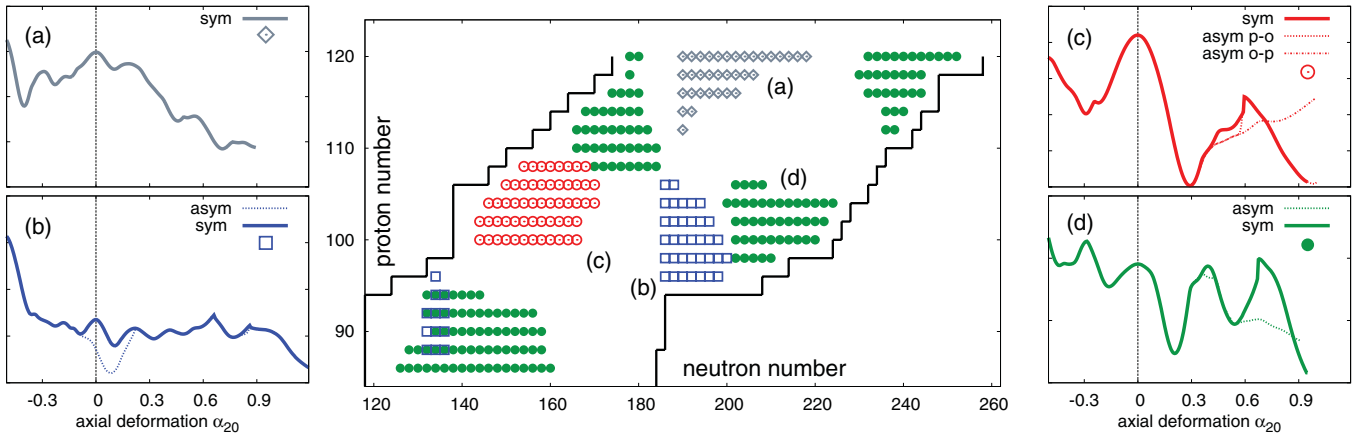

FIG. 4. (Color online) Schematic survey of fission modes for the various SHE. The two panels on the left and right show examples for the different regions as indicated: a) triaxial fission, b) asymmetrical ground-state energy, c) bi- or multimodal fission, d) asymmetric calculation removes completely the outer barrier.

$132 \leqslant N \leqslant 136$ and again in $96 \leqslant Z \leqslant 108$ and $186 \leqslant N \leqslant 198$. The breaking of reflection symmetry enhances the binding which, in turn, increases the fission barrier and thus leads to enhanced fission lifetime. This aspect will be discussed in more detail in the Appendix.

Panel c: shows a case where different fission paths emerge depending on whether one restricts the calculation on reflection symmetry or not or whether the calculation is going from oblate to prolate deformation or vice versa. This suggests a structure of two valleys where symmetric fission competes against asymmetric fission. This is also called multi- or bimodal fission and was already discussed in detail for self-consistent mean field models [25,31,62] as well as for the microscopic-macroscopic finite-range liquid-drop model [63] (and citations therein). A full multimodal treatment is presently beyond our possibilities. But the figure indicates that the barriers in the different channel are not so dramatically different. Thus it still provides a pertinent picture if we consider one particular path, the one along asymmetric shapes starting from outside.

Panel d: shows the standard case which has one unique barrier in asymmetric calculations. In order to demonstrate the effect of asymmetry we compare with the PES from reflection symmetric calculations. The latter show the double-humped fission barrier as it is known from actinides [64]. The allowance of asymmetric shapes removes the second barrier which holds for practically all SHE [21].

The overview demonstrates the large variety of topologies for the fission PES. This inhibits an automatic barrier search. Thus for the greater part of the investigated PES the minima and maxima relevant for the fission process were determined manually.

C. Systematics of fission barriers

A simple first indicator of fission instability is the height of the fission barrier. Figure 5 shows the systematics of fission barriers of SHE in the range $82 \leqslant Z \leqslant 120$ and $120 \leqslant N \leqslant 260$. All elements are found to be stable against immediate nucleon emission at the ground state and along the whole fission path. In case of a double-humped structure of the barrier (commonly appearing for $Z < 100$) the higher barrier is plotted. Results are shown for the four different Skyrme parametrizations SLy6, SkI3, SV-min, and SV-bas.

At first glance it is apparent that the Skyrme forces SkI3 and SLy6 yield notoriously much higher barriers as SV-min and SV-bas. This can be traced back to a difference in the

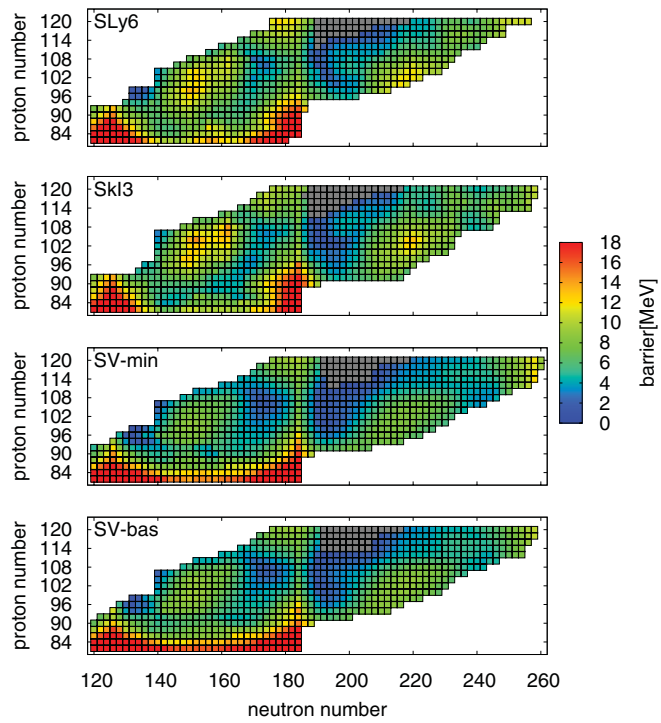

FIG. 5. (Color online) Systematics of fission barriers of even-even nuclei for four different Skyrme parametrizations SLy6 [40], SkI3 [33], SV-min [41], and SV-bas [41]. Grey indicates a possible triaxial fission, as already seen in Fig. 4.

effective mass m^*/m. SLy6 and SkI3 have a very low mass $m^*/m = 0.69$ and $m^*/m = 0.58$, respectively, while SV-bas and SV-min have effective masses 0.9 and 0.95. A low effective mass leads to a too low density of single-particle states, and thus to larger shell correction energies which, in turn, yield larger barriers.

All forces provide the same trends over the landscape of SHE. There is a strong variation in fission barriers corresponding to the strong variations of shell structure in the landscape of SHE. Several regions of high barriers occur. For low Z, i.e., Rn ($Z = 86$), Ra ($Z = 88$), and Th ($Z = 90$), one sees two islands of high barriers, one at $N \approx 126$ and another one at $N \approx 184$. Neutron numbers in between cover a region of lower barriers. They are particularly low for SkI3 and to some extend SLy6 while the fluctuations between high and low barriers are less dramatic for SV-bas and SV-min, corresponding to their generally smaller shell corrections. Stepping up to higher proton numbers Z there follow two more regions of high barriers, one of deformed SHE around $Z/N = 104/152$ and one of spherical SHE around $Z/N = 120/184$ (spherical shell closure). The magic neutron number N = 184 is clearly visible while an expected magic proton number near $Z = 120$ is indicated by a broad island of enhanced stability barriers around $Z/N = 120/184$ [18].

Considering the regime of nuclei relevant for r-process nucleosynthesis it is interesting to notice the appearance of a region of low fission barriers for $Z \sim 84$ in moving from $N = 126$ to $N = 184$ for SLy6 and particularly for SkI3. These low fission barriers may allow for neutron-induced fission to occur as the nucleosynthesis flow moves from the $N = 126$ region to the $N = 184$. The situation is different for SV-min and SV-mass, that predict much larger fission barriers in the r-process relevant region. For these parametrizations fission will only be relevant once the nucleosynthesis flow overcomes the $N = 184$ magic number. All four forces agree in predicting a rapid decrease of barrier heights going from the shell closure $N = 184$ up to neutron-rich nuclei. This suggest a substantial decrease in the production of nuclei beyond $N = 184$ during the r process. A more quantitative discussion requires to account for the competition between neutron induced fission and β decay, including β-delayed fission. This will be explored in a forthcoming publication.

To complete the picture, Fig. 6 shows results from four other models for which data are publicly available. The calculation were performed by using the extended Thomas-Fermi plus Strutinsky integral (ETFSI) [65], the Thomas-Fermi (TF) [66] method, the macroscopic-microscopic finite range liquid-drop model (FRDM) [63], or the SHF approach with the parametrization HFB14 [42]. All four theoretical mass models shows similar trends as observed in our studies. They confirm the region of high barriers below uranium, around neutron number $N = 184$ and the island around $Z/N = 104/152$, the latter, however, less strongly developed in case of TF and FRDM. The three non-self-consistent models (TF, ETFSI, FRDM) shift the third island of stability ($Z/N = 120/184$) down toward proton number $N = 114$. The rapid fall-off beyond $N = 184$ is confirmed. The case HFB14 belongs to the SHF family. In spite of the narrow range of results one can conclude that its systematics is very similar to the other

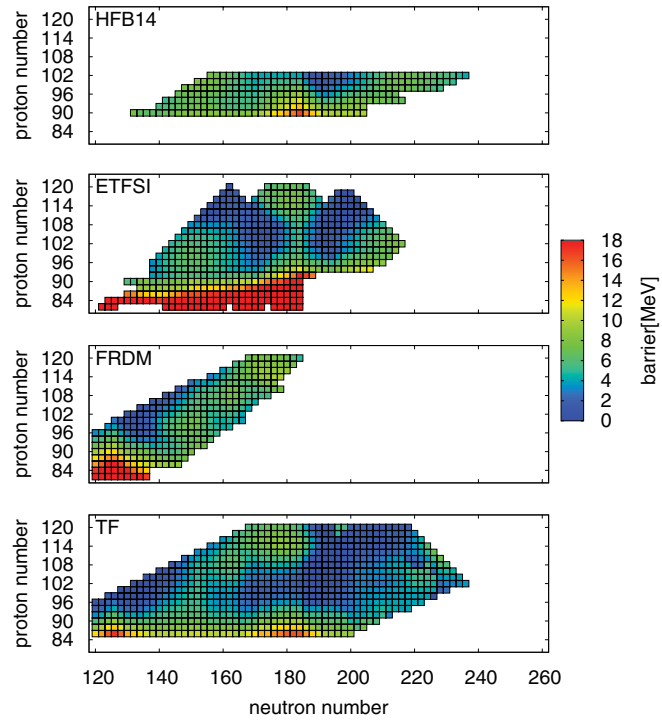

FIG. 6. (Color online) Results for fission barriers of four theoretical mass models HFB-14 [42], ETFSI [65], FRDM [63], TF [66] in the same region of nuclei. The shown data are reduced to even-even nuclei to enable a better comparison.

SHF cases. The actual barrier height are closer to SV-min and SV-bas (sometimes even below). This is not surprising as all models in Fig. 6 have a large effective mass, equals or around $m^*/m = 1$.

D. Fission lifetimes

Figure 7 shows fission lifetimes calculated with the recipe as outlined in Sec. II B in the range $100 \leqslant Z \leqslant 120$ and $140 \leqslant N \leqslant 260$ (from proton to neutron drip line) for the same Skyrme parametrizations as in the barrier systematics. Calculation of lifetimes were not performed for nuclei with proton numbers $Z \leqslant 98$, because the doubled humped barrier with the occurrence of fission isomers and transition states makes the evaluation of lifetimes for actinides cumbersome. SHE are simpler in that they have always one connected fission path (for an example see Fig. 10). The difference in barrier heights from 0 to 12 MeV (Fig. 5) translates to a difference in lifetimes from almost immediate decay to 10^{12} s and longer, demonstrating again the enormous sensitivity of fission lifetimes to all details of the model and computation.

At first glance, the basic pattern resemble much the systematics of barriers. Long-lived SHE are obviously found in the islands of high barriers. The island around $Z/N = 104/152$ is even broadened to higher Z and N toward the assumed neutron shell closure at $N = 162$, especially for SV-min and SV-bas. This demonstrates that not only barrier but also barrier width and collective mass can have a decisive influence. All

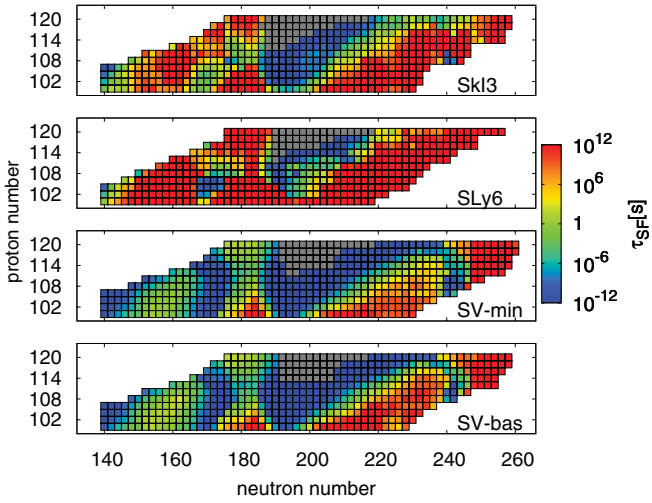

FIG. 7. (Color online) Systematics of fission lifetimes calculated in the range of proton numbers $100 \leqslant Z \leqslant 120$ and neutron numbers $140 \leqslant N \leqslant 260$ for even-even nuclei using the Skyrme parametrizations SkI3, SLy6, SV-min, and SV-bas.

parametrizations show a broad and deep valley of fission instability starting abrupt with neutron number $N = 186/188$. If the r-process nucleosynthesis flow is able to overcome the $N = 184$ magic number, it will proceed by the region of large spontaneous fission lifetimes in Fig. 5. However, once the neutrons are exhausted and matter β decays, the region of short spontaneous fission lifetimes will be reached and no long-lived SHE will be produced. The situation may be different for SkI3 and SLy6, depending on the extend of the region of short lifetimes above $Z > 120$.

There is a large difference between the SHF parametrizations in overall lifetime for elements with $N < 190$. The nuclei are much more stable for SkI3 and SLy6 than for SV-bas and SV-min. This is, of course, related to the overall difference in barrier heights (see Fig. 5) which can be traced back to different effective masses m^*/m. This produces here even a qualitative difference: The parametrizations SV-min and SV-bas show a valley of fission instability between the islands around $Z = 120$, $N = 180$, and $Z/N = 104/152$ while SkI3 and SLy6 do not. The immediate consequence is that SkI3 and SLy6 predict uninterrupted chains of α decay from the heaviest SHE down to actinides while SV-min and SV-bas have these α chains terminated by spontaneous fission. The latter is what is empirically found [5]. The competition with α decay is discussed in Sec. III E.

E. α decay

The α-decay half-lives are evaluated using the Viola-Seaborg relationship [67,68]:

$$\log(\tau_\alpha/\mathrm{s}) = (aZ + b)(Q_\alpha/\mathrm{MeV})^{-1/2} \quad (5)$$

$$+ (cZ + d) + h_{\log}, \quad (6)$$

$$a = 1.66175, \quad b = -0.5166, \quad (7)$$

$$c = -0.20228, \quad d = -33.9069, \quad (8)$$

$$Q_\alpha = E(N-2, Z-2) + E(2, 2) - E(N, Z)\,, \quad (9)$$

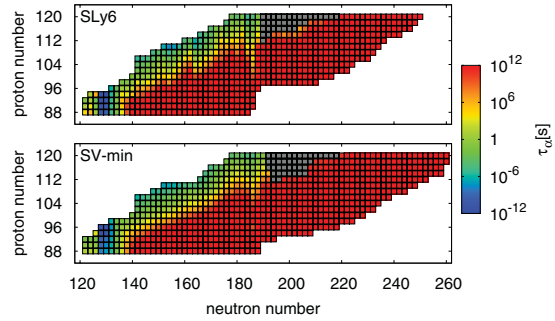

FIG. 8. (Color online) α-decay half-lives computed by using the Q_α values and the semi empirical Viola-Seaborg formula.

$$E(2, 2) = E_{\exp}(^4\mathrm{He}) = 28.3\ \mathrm{MeV}, \quad (10)$$

and $h_{\log} = 0$ for the even-even nuclei considered here. This requires as only input the Q_α values which can be determined easily as difference of ground state binding energies. The latter are computed allowing for axial deformations as well as reflection-symmetry breaking and including approximate angular momentum projection for deformed nuclei. It is to be noted that the difference of binding energies, as the Q_α value, are predicted rather reliably with the SHF models although the binding energies as such are notoriously underestimated for SHE [41,59].

Figure 8 shows the systematics of α-decay half-lives calculated with the SHF parametrizations SLy6 and SV-min. In contrast to fission lifetimes, α-decay half-lives vary in general smoothly and steadily with a tendency to increase when going in direction of neutron rich SHE. An exception are the spherical neutron shell closures at $N = 126$ and $N = 184$ which are clearly marked by a sudden decrease of α half-lives. But there is no detailed structure like the islands of stable nuclei in spontaneous fission systematics. Most of the nuclei in the shown region are very stable against α decay. It is only the band of neutron-deficient SHE at the left side of the region where α decay plays a role as competitor to fission and β decay. Comparing with the fission lifetimes in Fig. 7 that α decay prevails in any case for the islands of fission stability around $Z = 120$, $N = 180$, and $Z/N = 104/152$. The parametrizations SV-min and SV-bas produce the pronounced valley of fission instability between these islands for which then fission takes the lead over α decay. This does not happen for SLy6 and SkI3 with their generally longer fission lifetimes.

A direct comparison of α decay and fission is provided in Fig. 9 showing the systematics of the dominant decay channels. Results are shown for the two parametrizations SV-min and SLy6 and compared with data. The experimental situation is just in between the two theoretical predictions. SLy6 produces too much fission stability thus giving α decay too much dominance while SV-min slightly underestimates the impact of α decay. Consider the α decay chain from $Z = 118$, $N = 176$. It is terminated by fission already for $Z = 116$ for SV-min while the experimental chain terminates later at $Z = 112$. The results for SkI3 are very similar to those of SLy6 and the results for SV-bas to those of SV-min.

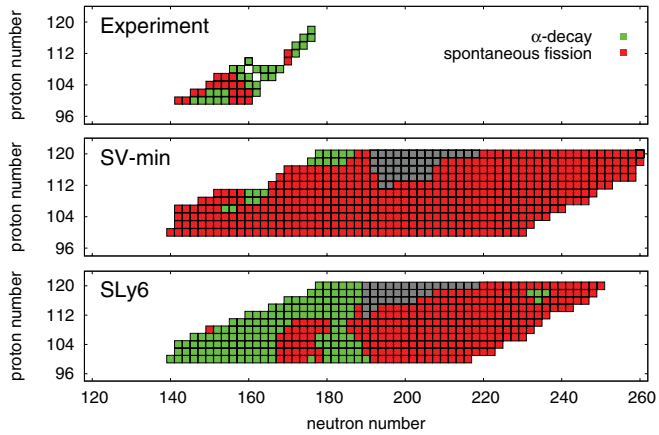

FIG. 9. (Color online) Minimal lifetime plots for the competing decay channels α decay and spontaneous fission. Experimental known decay channels [50] are compared to results using the parametrization SV-min and SLy6.

It is to be noticed that the trends which are seen here in the systematics had already been spotted in Fig. 3. The parametrizations SV-min and SV-bas perform generally better, but are still plagued by producing a wrong trend when stepping to the heavier end of SHE where they yield too low barriers and lifetimes. A better compromise has yet to be worked out.

IV. CONCLUSIONS

We have explored the systematics of fission barriers and lifetimes in the realm of superheavy elements (SHE) on the grounds of self-consistent calculations using the Skyrme-Hartree-Fock (SHF) approach. The fission path has been generated with a quadrupole constraint producing a series of axially symmetric deformations while allowing for reflection-asymmetric shapes. The corresponding collective mass is computed by self-consistent cranking (often called ATDHF cranking). The quantum corrections to the collective potential (angular momentum projection, vibrational zero-point energy) are properly taken into account. The fission life-time is computed for thus given potential and mass by the semiclassical WKB approximation, while the ground state energy, which is at the same time the entrance energy for fission, is computed quantum mechanically in the given collective geometry of one axial deformation plus two rotation angles. Results have been produced for a couple of different SHF parametrizations to explore the sensitivity to the parametrization. For comparison, we have also computed the α-decay lifetimes using the Viola systematics.

A first test was performed by comparing with known fission lifetimes in isotopic chains in the lower region of superheavy elements, $Z = 104$–108 and for the few available data points in even heavier elements. The span of predictions is large whereby the effective mass of the underlying parametrization plays a crucial role. Satisfying agreement is found for modern parametrizations using effective mass around $m^*/m = 0.9$–1. There remains, however, one open problem with the global trend: The parametrizations which perform almost perfectly in the region $Z = 104$–108 underestimate fission barriers and lifetimes in the heavier region $Z = 112$ and 114.

The landscape of SHE separates into regions of different topology of the fission path. The most widely found standard case is a unique, axially symmetric fission path showing only one fission barrier; the second barrier which is known from actinides is suppressed by reflection asymmetric shapes which regularly develop for larger deformations. Proton rich isotopes in $100 \leqslant Z \leqslant 108$ show often a tendency to bi- or multimodal fission where different fission and fusion paths compete. A small region around $Z = 118$ and $N = 200$ has oblate (if not triaxial) ground states and can decay only through a manifestly triaxial fission path. There are, furthermore, two small regions where the ground state is reflection asymmetric. This was shown to enhance barrier and lifetimes at a quantitative level, but not changing the global trends.

The systematics of fission barriers and lifetimes shows the known islands of stability around $Z/N = 104/152$ in the region of a deformed shell closure and around $Z/N = 118/178$ in a region of spherical isotopes. The actual values of barriers and lifetimes depend very much on the SHF parametrizations. Those with low effective mass (here SkI3 and SLy6) produce very high barriers and lifetimes while those with high effective mass (SV-min and SV-bas) yield moderate barriers and lifetimes. The latter group also produces a valley of fission instability between the two islands, qualitatively in accordance with the empirical findings. The way to very neutron rich r-process nuclei with $N > 184$ starts out with a large region of fission instability. Some stability is gained at the extremely neutron rich end. This makes unlikely the production of long-lived SHE above $Z = 100$ by the r process. However, a more realistic estimate of the production of SHE by the r process will require nucleosynthesis calculations based on the present barriers and lifetimes. This will be the subject of a forthcoming publication.

We have also computed α-decay lifetimes using the Viola-Seaborg formula. While the fission lifetimes show dramatic variation over the chart of superheavy elements (from instability to $\tau_{\text{fiss}} = 10^{16}$ s), the α-decay times vary gently with small overall changes and without visible shell effects. The general crossover from α decay to fission along the decay chains from the upper island of SHE is qualitatively reproduced by the family of SHF parametrizations with high effective mass. A quantitatively reliable prediction of the switching point is detail on which the models have yet to be refined.

ACKNOWLEDGMENTS

This work was supported by the BMBF under Contract No. 06 ER 9063, by the Office of Nuclear Physics, US Department of Energy under Contract Nos. DE-FG02-96ER40963 and DE-FC02-09ER41583, by the ExtreMe Matter Institute EMMI in the framework of the Helmholtz Alliance HA216/EMMI, by the Deutsche Forschungsgemeinschaft through contract SFB 634, by the Helmholtz Internation Center for FAIR

within the framework of the LOEWE program launched by the state of Hesse and by the Helmholtz Association through the Nuclear Astrophysics Virtual Institute (VH-VI-417). We thank H. Feldmeier and F.-K. Thielemann for valuable discussions.

APPENDIX A: SYMMETRIC VS. ASYMMETRIC (INCLUDING ISOMER)

Reflection asymmetric shapes are a key issue in fission of SHE and thus have been much debated under different aspects as, e.g., suppression of the second barrier, impact of ground state asymmetry on the first barrier, or influence on bi- and multimodal fission [31,62,63,69]. We will discuss here the effect of reflection asymmetric ground states on the fission barrier and subsequently on lifetimes.

Figure 10 shows the PES of the two isotopes ^{286}Rf and ^{294}Rf. In the majority of the cases symmetric and asymmetric calculations provide the same ground state energy. This is illustrated by ^{286}Rf. In contrast, for ^{294}Rf the asymmetric calculation yields an energetically more favorable ground state (around $\alpha_{20} = 0.08$), while in the symmetric PES it is difficult to locate the minimum (possibly around $\alpha_{20} = 0.32$). It is to be remarked that the tendency to symmetry breaking is confined to the ground state region thus lowering the ground state energy. The absolute height of the barrier remains almost unaffected. As a consequence, an asymmetric ground state will lead to higher (relative) fission barriers.

Besides Rf, the elements Pu, U, Th, R, and Rn are also known for the importance of the octupole degree of freedom [70,71]. Figure 11 summarizes for all relevant elements the differences of binding energies and fission barriers between

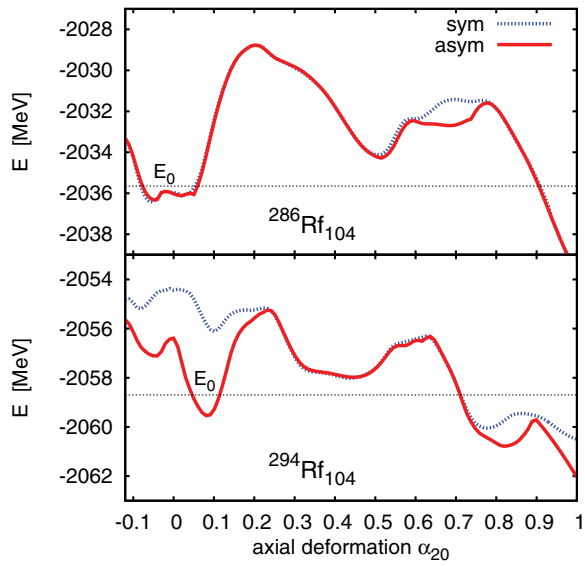

FIG. 10. (Color online) PES of the isotopes ^{294}Rf and ^{294}Rf for symmetric and asymmetric shapes calculated with the Skyrme parametrization SLy6. The fission path is indicated by a faint horizontal line.

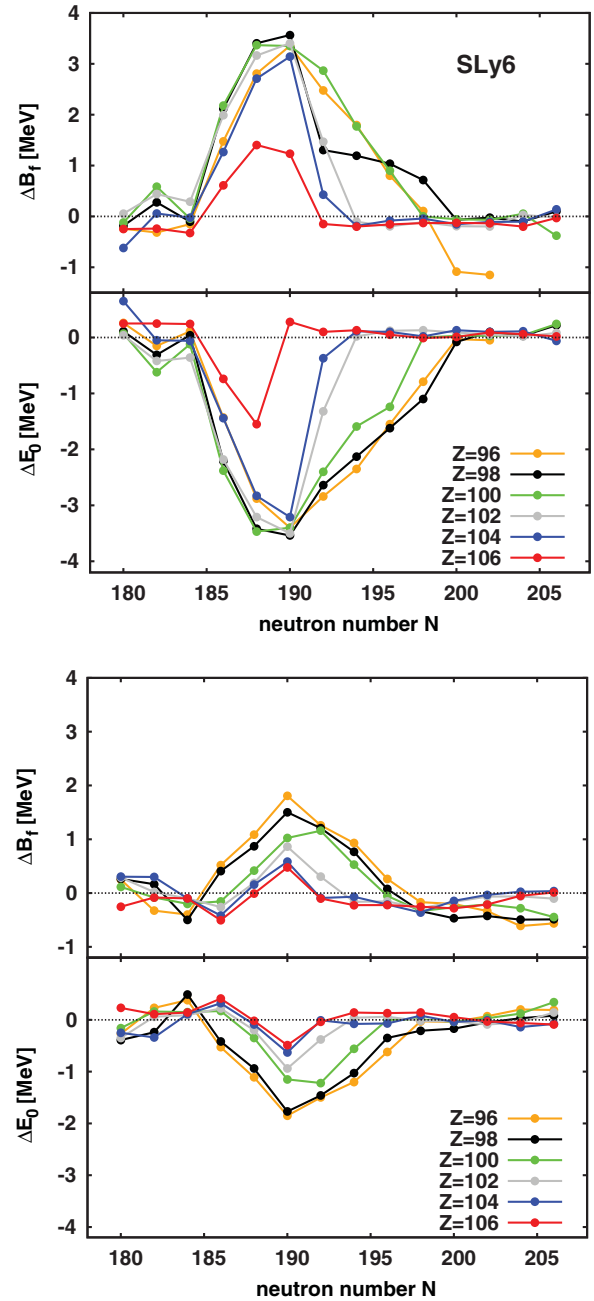

FIG. 11. (Color online) Difference of ground state energies ΔE_0 and fission barriers δB_f between reflection symmetric and asymmetric calculations for the isotopes as indicated. The upper panels show results computed with the Skyrme parametrization SLy6 and the lower panels with SV-min.

reflection symmetric and asymmetric calculations for SLy6 (upper panels) and SV-min (lower panels). All these isotopes display basically the effect as discussed for Rf, namely that the asymmetric shape affects predominantly the ground state thus leading to an increase in the fission barrier which corresponds directly to the lowering of the ground state. The size of the effect changes quickly with proton and neutron number which is no surprise because symmetry breaking is driven by (quickly

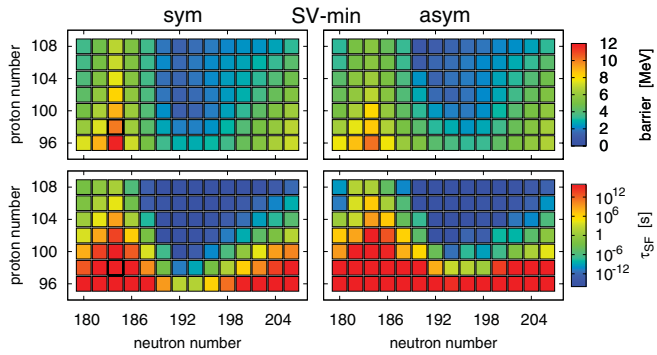

FIG. 12. (Color online) Comparison of symmetric and asymmetric fission barriers and half-lives in region b) of the schematic survey Fig. 4 where asymmetric ground states can play a role. The upper panels show barriers and the lower panels lifetimes. The left panels show results from reflection symmetric calculations and the right panels from calculations where asymmetric shapes were allowed. The results are calculated with the parametrization SV-min.

changing) shell structure. This also explains that the results from SLy6 and SV-min are quantitatively so much different. SLy6 has a significantly lower effective mass than SV-min thus lower level density and, in turn, larger shell corrections. The lowering of the ground-state energy was also investigated using other Skyrme forces [72], where the results show a strong dependence on the effective mass m^*/m and the pairing strength. A small effective mass or a small pairing strength lead to a big effect on the ground state energy and vice versa.

Figure 12 compares the systematics of barriers (upper panels) and lifetimes (lower panels) with and without allowing for asymmetric shapes in the region of relevant isotopes. One spots a slightly increased fission stability in case of allowed asymmetry in the feature that the stable regions are somewhat extended. However, the overall trends and the general impression of the plots of systematics remains the same. The effect of asymmetric shapes appears rather at a quantitative level. The example demonstrates how robust the analysis of global trends is.

[1] J. R. Nix, Annu. Rev. Nucl. Sci. **22**, 66 (1972).
[2] S. Hofmann and G. Münzenberg, Rev. Mod. Phys. **72**, 733 (2000).
[3] S. Hofmann, F. Heßberger, D. Ackermann, S. Antalic, P. Cagarda, S. Ćwiok, B. Kindler, J. Kojouharova, B. Lommel, R. Mann, G. Münzenberg, A. Popeko, S. Saro, H. Schtt, and A. Yeremin, Eur. Phys. J. A **10**, 5 (2001).
[4] Y. T. Oganessian, V. K. Utyonkov, Y. V. Lobanov, F. S. Abdullin, A. N. Polyakov, I. V. Shirokovsky, Y. S. Tsyganov, G. G. Gulbekian, S. L. Bogomolov, B. N. Gikal, A. N. Mezentsev, S. Iliev, V. G. Subbotin, A. M. Sukhov, A. A. Voinov, G. V. Buklanov, K. Subotic, V. I. Zagrebaev, M. G. Itkis, J. B. Patin, K. J. Moody, J. F. Wild, M. A. Stoyer, N. J. Stoyer, D. A. Shaughnessy, J. M. Kenneally, P. A. Wilk, R. W. Lougheed, R. I. Il'kaev, and S. P. Vesnovskii, Phys. Rev. C **70**, 064609 (2004).
[5] Y. T. Oganessian, V. K. Utyonkov, Y. V. Lobanov, F. S. Abdullin, A. N. Polyakov, R. N. Sagaidak, I. V. Shirokovsky, Y. S. Tsyganov, A. A. Voinov, G. G. Gulbekian, S. L. Bogomolov, B. N. Gikal, A. N. Mezentsev, S. Iliev, V. G. Subbotin, A. M. Sukhov, K. Subotic, V. I. Zagrebaev, G. K. Vostokin, M. G. Itkis, K. J. Moody, J. B. Patin, D. A. Shaughnessy, M. A. Stoyer, N. J. Stoyer, P. A. Wilk, J. M. Kenneally, J. H. Landrum, J. F. Wild, and R. W. Lougheed, Phys. Rev. C **74**, 044602 (2006).
[6] K. E. Gregorich, J. M. Gates, C. E. Düllmann, R. Sudowe, S. L. Nelson, M. A. Garcia, I. Dragojević, C. M. Folden III, S. H. Neumann, D. C. Hoffman, and H. Nitsche, Phys. Rev. C **74**, 044611 (2006).
[7] J. Dvorak, W. Brüchle, M. Chelnokov, C. E. Düllmann, Z. Dvorakova, K. Eberhardt, R. Eichler, E. Jäger, R. Krücken, A. Kuznetsov, Y. Nagame, F. Nebel, K. Nishio, R. Perego, Z. Qin, M. Schädel, B. Schausten, E. Schimpf, R. Schuber, A. Semchenkov, P. Thörle, A. Türler, M. Wegrzecki, B. Wierczinski, A. Yakushev, and A. Yeremin, Phys. Rev. Lett. **100**, 132503 (2008).
[8] G. Martínez-Pinedo, D. Mocelj, N. Zinner, A. Keli, K. Langanke, I. Panov, B. Pfeiffer, T. Rauscher, K.-H. Schmidt, and F.-K. Thielemann, Prog. Part. Nucl. Phys. **59**, 199 (2007).
[9] M. Arnould, S. Goriely, and K. Takahashi, Phys. Rep. **450**, 97 (2007).
[10] J. Stone and P.-G. Reinhard, Prog. Part. Nucl. Phys. **58**, 587 (2007).
[11] P. Ring, Prog. Part. Nucl. Phys. **37**, 193 (1996).
[12] M. Bender, P.-H. Heenen, and P.-G. Reinhard, Rev. Mod. Phys. **75**, 121 (2003).
[13] D. Vretenar, A. Afanasjev, G. Lalazissis, and P. Ring, Phys. Rep. **409**, 101 (2005).
[14] J. Erler, P. Klüpfel, and P.-G. Reinhard, J. Phys. G **38**, 033101 (2011).
[15] M. Brack, J. Damgård, A. S. Jensen, H. C. Pauli, V. M. Strutinsky, and C. Y. Wong, Rev. Mod. Phys. **44**, 320 (1972).
[16] M. Bender, K. Rutz, P.-G. Reinhard, J. A. Maruhn, and W. Greiner, Phys. Rev. C **60**, 034304 (1999).
[17] A. T. Kruppa, M. Bender, W. Nazarewicz, P.-G. Reinhard, T. Vertse, and S. Ćwiok, Phys. Rev. C **61**, 034313 (2000).
[18] M. Bender, W. Nazarewicz, and P.-G. Reinhard, Phys. Lett. **515**, 42 (2001).
[19] H. J. Specht, Rev. Mod. Phys. **46**, 773 (1974).
[20] H. Flocard, P. Quentin, D. Vautherin, M. Véneroni, and A. K. Kerman, Nucl. Phys. A **231**, 176 (1974).
[21] T. Bürvenich, M. Bender, J. A. Maruhn, and P.-G. Reinhard, Phys. Rev. C **69**, 014307 (2004).
[22] J. Bartel, P. Quentin, M. Brack, C. Guet, and H.-B. Håkansson, Nucl. Phys. A **386**, 79 (1982).
[23] P.-G. Reinhard and K. Goeke, Rep. Prog. Phys. **50**, 1 (1987).
[24] P.-G. Reinhard, Nucl. Phys. A **261**, 291 (1976).
[25] M. Bender, K. Rutz, P.-G. Reinhard, J. A. Maruhn, and W. Greiner, Phys. Rev. C **58**, 2126 (1998).
[26] Y. T. Oganessian , V. K. Utyonkov, Y. V. Lobanov, F. S. Abdullin, A. N. Polyakov, I. V. Shirokovsky, Y. S. Tsyganov, G. G. Gulbekian, S. L. Bogomolov, B. N. Gikal, A. N. Mezentsev, S. Iliev, V. G. Subbotin, A. M. Sukhov, G. V. Buklanov, K. Subotic, M. G. Itkis, K. J. Moody, J. F. Wild, N. J. Stoyer, M. A. Stoyer, and R. W. Lougheed, Phys. Rev. Lett. **83**, 3154 (1999).
[27] Y. T. Oganessian, N. Rowley, Nature **400**, 209 (1999).

[28] Y. T. Oganessian Yu. Ts. Oganessian, V. K. Utyonkov, Yu. V. Lobanov, F. Sh. Abdullin, A. N. Polyakov, I. V. Shirokovsky, Yu. S. Tsyganov, G. G. Gulbekian, S. L. Bogomolov, B. N. Gikal, A. N. Mezentsev, S. Iliev, V. G. Subbotin, A. M. Sukhov, O. V. Ivanov, G. V. Buklanov, K. Subotic, M. G. Itkis, K. J. Moody, J. F. Wild, N. J. Stoyer, M. A. Stoyer, R. W. Lougheed, C. A. Laue, Ye. A. Karelin, and A. N. Tatarinov, Phys. Rev. C **63**, 011301(R) (2000).

[29] J. F. Berger, L. Bitaud, J. Decharg, M. Girod, and K. Dietrich, Nucl. Phys. **685**, 1 (2001).

[30] M. Warda, J. Egido, and L. Robledo, Phys. Scr., T **125**, 226 (2006).

[31] A. Staszczak, A. Baran, J. Dobaczewski, and W. Nazarewicz, Phys. Rev. C **80**, 014309 (2009).

[32] N. Schindzielorz, J. Erler, P. Klüpfel, P.-G. Reinhard, and G. Hager, Int. J. Mod. Phys. E **18**, 773 (2009).

[33] P.-G. Reinhard and H. Flocard, Nucl. Phys. A **584**, 467 (1995).

[34] S. J. Krieger, P. Bonche, H. Flocard, P. Quentin, and M. S. Weiss, Nucl. Phys. A **517**, 275 (1990).

[35] J. Dobaczewski, W. Nazarewicz, and P.-G. Reinhard, Nucl. Phys. **693**, 361 (2001).

[36] J. Erler, P. Klüpfel, and P.-G. Reinhard, Eur. Phys. J. A **37**, 81 (2008).

[37] M. Bender, K. Rutz, P.-G. Reinhard, and J. A. Maruhn, Eur. Phys. J. A **8**, 59 (2000).

[38] P.-G. Reinhard, W. Nazarewicz, M. Bender, and J. A. Maruhn, Phys. Rev. C **53**, 2776 (1996).

[39] J. W. Negele and D. Vautherin, Phys. Rev. C **5**, 1472 (1972).

[40] E. Chabanat, P. Bonche, P. Haensel, J. Meyer, and R. Schaeffer, Nucl. Phys. A **635**, 231 (1998); **643**, 441(E) (1998).

[41] P. Klüpfel, P.-G. Reinhard, T. J. Bürvenich, and J. A. Maruhn, Phys. Rev. C **79**, 034310 (2009).

[42] S. Goriely, S. Hilaire, A.J. Koning, M. Sin, and R. Capote, Phys. Rev. C **79**, 024612 (2009).

[43] G. D. Dang, A. Klein, and N. R. Walet, Phys. Rep. **335**, 93 (2000).

[44] P. Möller, J. R. Nix, and W. J. Swiatecki, Nucl. Phys. **469**, 1 (1987).

[45] R. Smolańczuk, J. Skalski, and A. Sobiczewski, Phys. Rev. C **52**, 1871 (1995).

[46] P. Klüpfel, J. Erler, P.-G. Reinhard, and J. Maruhn, Eur. Phys. J. A **37**, 343 (2008).

[47] P.-G. Reinhard, Z. Phys. A **285**, 93 (1978).

[48] K. Hagino, P.-G. Reinhard, and G. F. Bertsch, Phys. Rev. C **65**, 064320 (2002).

[49] S. Ćwiok, J. Dobaczewski, P.-H. Heenen, P. Magierski, and W. Nazarewicz, Nucl. Phys. A **611**, 211 (1996).

[50] G. Audi, O. Bersillon, J. Blachot, and A. H. Wapstra, Nucl. Phys. A **729**, 3 (2003).

[51] J. Khuyagbaatar, S. Hofmann, F. Heßberger, D. Ackermann, H. Burkhard, S. Heinz, B. Kindler, I. Kojouharov, B. Lommel, R. Mann, J. Maurer, K. Nishio, and Y. Novikov, Eur. Phys. J. A **37**, 177 (2008).

[52] D. Peterson, B. B. Back, R. V. F. Janssens, T. L. Khoo, C. J. Lister, D. Seweryniak, I. Ahmad, M. P. Carpenter, C. N. Davids, A. A. Hecht, C. L. Jiang, T. Lauritsen, X. Wang, S. Zhu, F. G. Kondev, A. Heinz, J. Qian, R. Winkler, P. Chowdhury, S. K. Tandel, and U. S. Tandel, Phys. Rev. C **74**, 014316 (2006).

[53] Y. T. Oganessian, V. K. Utyonkov, Y. V. Lobanov, F. S. Abdullin, A. N. Polyakov, I. V. Shirokovsky, Y. S. Tsyganov, A. N. Mezentsev, S. Iliev, V. G. Subbotin, A. M. Sukhov, K. Subotic, O. V. Ivanov, A. N. Voinov, V. I. Zagrebaev, K. J. Moody, J. F. Wild, N. J. Stoyer, M. A. Stoyer, and R. W. Lougheed, Phys. Rev. C **64**, 054606 (2001).

[54] J. M. Gates, M. A. Garcia, K. E. Gregorich, C. E. Düllmann, I. Dragojević, J. Dvorak, R. Eichler, C. M. Folden, W. Loveland, S. L. Nelson, G. K. Pang, L. Stavsetra, R. Sudowe, A. Türler, and H. Nitsche, Phys. Rev. C **77**, 034603 (2008).

[55] S. Hofmann, F. P. Heßberger, D. Ackermann, S. Antalic, P. Cagarda, S. Ćwiok, B. Kindler, J. Kojouharova, B. Lommel, R. Mann, G. Münzenberg, A. G. Popeko, S. Saro, H. J. Schoİtt, and A. V. Yeremin, Eur. Phys. J. A **10**, 5 (2001).

[56] S. K. Tandel, T. L. Khoo, D. Seweryniak, G. Mukherjee, I. Ahmad, B. Back, R. Blinstrup, M. P. Carpenter, J. Chapman, P. Chowdhury, C. N. Davids, A. A. Hecht, A. Heinz, P. Ikin, R. V. F. Janssens, F. G. Kondev, T. Lauritsen, C. J. Lister, E. F. Moore, D. Peterson, P. Reiter, U. S. Tandel, X. Wang, and S. Zhu, Phys. Rev. Lett. **97**, 082502 (2006).

[57] M. G. Itkis, Y. T. S. Oganessian, and V. I. Zagrebaev, Phys. Rev. C **65**, 044602 (2002).

[58] J. Péter, Eur. Phys. J. A **22**, 271 (2004).

[59] J. Erler, P. Klüpfel, and P.-G. Reinhard, J. Phys. G **37**, 064001 (2010).

[60] J. Erler, P. Klüpfel, and P.-G. Reinhard, Phys. Rev. C **82**, 044307 (2010).

[61] M. Bender and P.-G. Reinhard, GSI scientific report 2000, document "Nuc St/52" (GSI Darmstadt, April 2001).

[62] M. Warda, J. L. Egido, L. M. Robledo, and K. Pomorski, Phys. Rev. C **66**, 014310 (2002).

[63] P. Möller, A. J. Sierk, T. Ichikawa, A. Iwamoto, R. Bengtsson, H. Uhrenholt, and S. Åberg, Phys. Rev. C **79**, 064304 (2009).

[64] S. Bjørnholm and J. E. Lynn, Rev. Mod. Phys. **52**, 725 (1980).

[65] A. Mamdouh, J. Pearson, M. Rayet, and F.Tondeur, Nucl. Phys. A **679**, 337 (2001).

[66] W. D. Myers and W. J. Swiatecki, Phys. Rev. C **60**, 014606 (1999).

[67] V. Viola and G. Seaborg, J. Inorg. Nucl. Chem. **28**, 741 (1966).

[68] A. Sobiczewski, Z. Patyk, and S. Ćwiok, Phys. Lett. B **224**, 1 (1989).

[69] L. Bonneau, Phys. Rev. C **74**, 014301 (2006).

[70] W. Nazarewicz, P. Olanders, I. Ragnarsson, J. D. G. Leander, P. Möller, and E. Ruchowsa, Nucl. Phys. A **429**, 269 (1984).

[71] J. L. Egido and L. M. Robledo, Nucl. Phys. A **524**, 65 (1991).

[72] H. Loens, Ph.D. thesis, Technische Universiät Darmstadt, Darmstadt, 2011.